Journal of Molecular Structure 1251 (2022) 132061

Contents lists available at ScienceDirect

Journal of Molecular Structure

journal homepage: www.elsevier.com/locate/molstr

Ho^{3+}activated $Ca_{0.5}Y_{1.90-x}O_3$ green-emitting nanophosphors for solid state lightening: Synthesis, characterization and photoluminescence properties

Arpita Dwivedi[a], Monika Srivastava[b], S.K. Srivastava[a,*]

[a] Department of Physics, Institute of Science, Banaras Hindu University, Varanasi 221005, India
[b] School of Materials Science and Technology, IIT (BHU), Varanasi 221005, India

ARTICLE INFO

Article history:
Received 1 November 2021
Revised 26 November 2021
Accepted 28 November 2021
Available online 30 November 2021

Keywords:
Photoluminescence
Ho^{3+} ions
Nanophosphor
Combustion
CIE

ABSTRACT

This paper presents a series of Ho^{3+}activated $Ca_{0.5}Y_{1.90-x}O_3$ green-emitting nanophosphors using the facile solution combustion method. X-ray diffraction (XRD) and Transmission electron microscope (TEM) confirm the phase purity, structural morphology with cubic phase, and irregular shape particle with the average particle size of 21 nm. Diffuse reflectance spectra of the recorded and band gap estimated by Tauc's equation which is 5.78 eV, 4.90 eV for direct and indirect band gaps for 2 mol% of Ho^{3+}, respectively. Under the excitation of 448 nm wavelength ($^5I_8 \rightarrow {}^3G_6$), the doped samples display characteristic emission of Ho^{3+} ions correspond to $^5S_2 \rightarrow {}^5I_8$ (at 551 nm) transition, which fall in a strong green region. The optimal concentration for Ho^{3+} doping is found as 2 mol%, after this quenching of photoluminescence (PL) intensity occurred and this is accredited due to dipole-dipole interaction. The proposed nanophosphor also displays the good thermal stability with activation energy of 0.23 eV. The nanophosphor confirms the excellent color purity (98%), CRI (98.36%), and CCT value (5724 K). With this, nanophosphor also exhibits good quantum efficiency of 81.1% under the 448 nm excitation wavelength. These results direct that the Ho^{3+}activated $Ca_{0.5}Y_{1.90-x}O_3$ nanophosphor may have potential applicability for green-emitting LEDs, display device and optoelectronic applications.

1. Introduction

Nowadays, there is huge demand for highly efficient LEDs and display devices, which have less power consumption properties. Rare earth doped inorganic materials are considered superior as they can provide narrow emission with UV excitation. This property makes it available for various fields like in lamp industry, color display, medical imaging, laser and security devices etc. [1–3]. For the lamp industries the rare earth doped phosphor material gained much attention for fabrication of the light emitting diodes (LEDs). Hence, for realizing an efficient LED, phosphor material must have good luminescence efficiency, narrow emission and high color rendering index which define it an efficient material for optoelectronic applications [4–6]. Generally, rare earth doped material has all these properties and is used as activator ions, because it has forbidden 4f-4f transitions for the same parity and does not follow the Laporte selection rules. However, doping with the non-centrosymmetric state with opposite parity ligands, leads to parity allowed transitions. These result in the emission in a narrow band, as 4f electrons of rare-earth ions are shielded by large $5s^25p^6$ radial subshells [6,7].

In various activator rare earth ions, holmium (Ho^{3+}) ions are an important activator ion as it has a broad PL spectrum from visible to IR range with strong green emission [2,6,8]. For the Ho^{3+} ions green emission dominant due to $^5F_4$; $^5S_2 \rightarrow {}^5I_8$ transitions over the blue and red emission, this is also mentioned in the Singh et al. [5] and Atabaev et al. [8]. The efficient green emission of Ho^{3+} ions can be applicable in various fields like solid state lighting devices, field emission display, security printing and for biological and sensing applications [3,4,9]. To obtain an efficient phosphor it is important to select a proper host and Y_2O_3 are the most suitable host for doping with rare earth. As the Y_2O_3 has similar chemical and physical properties with various rare earth ions such as large transparency range and also have similar ionic radii, high melting point minimum and thermal expansion coefficient[8]. Rare earth doped Y_2O_3 also has a wide range of applications [10,11]. Further, to improve luminescence qualities co-doping can be done, which can be used as a sensitizer by effectively transferring en-

* Corresponding author.
E-mail address: sanjay_itbhu@yahoo.com (S.K. Srivastava).

https://doi.org/10.1016/j.molstruc.2021.132061
0022-2860/

ergy to the activator rare earth ions (Ho^{3+}). Sometimes co-doping generates defects which improve the luminescence property of the material with high quantum efficiency. There is various work which shows the co-doping enhances the luminance intensity by increasing transition probability [9,12]. The monovalent ions (Li^{+}, Na^{+}, K^{+}) and divalent ions (Ca^{2+}, Sr^{2+}, Mg^{2+}) are widely used as a common co-dopant material to improve the performance of phosphor material by enhancing PL intensity [9,10]. The divalent ions (Ca^{2+}, Sr^{2+}, Mg^{2+}) and rare-earth ions have different valence states, which affect the lattice structure, creates distortion in the crystal field of rare earth ions and improve the optical properties of the phosphor material [13]. Kumari, Manam reported the improvement of PL emission intensity of YVO_4:Eu^{3+} after doping with alkaline earth metal ion [12]. Shi, et al. reported the effect of doping of divalent ions with Eu^{3+}:Y_2O_3 [9]. However, doping with divalent ions with Ho^{3+} is less focused and studied and no detailed analysis with Ho^{3+} doped $Ca_{0.5}Y_{1.90-x}O_3$ nanophosphor has been studied so far.

The present work reports the effect of doping concentration of Ho^{3+} ions on the structural and optical properties of $Ca_{0.5}Y_{1.90-x}O_3$:xHo^{3+} nanophosphor. The samples of $Ca_{0.5}Y_{1.90-x}O_3$:xHo^{3+} nanophosphor is synthesis by solution combustion method using urea as a fuel, as best of our knowledge this combination of $Ca_{0.5}Y_{1.90-x}O_3$:xHo^{3+} phosphor material has not been investigated and reported yet. To study phase purity, structural and morphological characterization were carried out by X-ray diffraction (XRD) and Transmission electron microscope (TEM), respectively. Purity of the sample has been tested by FTIR. The optical properties are investigated through photoluminescence spectra and diffuse reflectance spectra (DRS). The optical band gap of the phosphor materials is also calculated from DRS. The decay lifetime corresponding to the $^5S_2$ state of different concentrations of Ho^{3+} was also studied and described. The photometric properties and color purity has been also studied using a chromaticity diagram. The energy transfer mechanism with an energy level diagram is also discussed.

2. Experimental method

2.1. Materials and synthesis

The starting material yttrium oxide (Y_2O_3), calcium oxide (CaO), and holmium oxide (Ho_2O_3), was purchased from Sigma-Aldrich. Urea (NH_2CONH_2) and nitric acid (HNO_3) was perched from Loba Chemie all are analytical and used without further purifications. A series of $Ca_{0.5}Y_{1.90-x}O_3$:xHo^{3+} (x = 0.05, 1, 1.5, 2, 2.5, 3 mole%) nanophosphor was synthesised by solution combustion method according to the solution:

$$nHo(NO_3)_3 + 0.5Ca(NO_3)_2 + (2 - x - 0.5)[Y(NO_3)_3] + NH_2CONH_2 + H_2O \rightarrow Ca_{0.5}Y_{(1.90-x)}Ho_xO_3 + H_2O \uparrow + CO_2 \uparrow + \text{other gaseous product}$$

For the synthesis, stoichiometric amounts of Y_2O_3, Ho_2O_3, and CaO reagents are mixed separately with the 2 ml HNO_3 and mixed separately in beakers until a transparent solution of it. Next, a separate solution of urea (used as fuel) with 10 ml deionised water (in 2:1 urea to metal ion ratio) was formed. The nitrate solution of all the reagents is mixed with solution of urea in a beaker followed by continuous starting of 30 min. Further, the obtained transparent mixture was kept in the furnish at 600 °C for 1 hour. Finally, we get a white powder cooled to room temperature gridded and washed twice with ethanol followed by calcination at 900 °C for 8 h and used for further characterizations.

2.2. Characterizations

X-ray diffraction of the synthesised sample was recorded through (XRD-Rigaku Mini Flax 600 diffractometer) with CuK_α radiation (λ = 1.54,046 Å) for the 2θ range 10°−80° at scan rate 0.02°/min. The BRUKER-ALPHA II FT-IR spectrometer was used to record Fourier transform infrared (FTIR). The morphological and microstructures characterization of the synthesized material was estimated through transmission electron microscope (TEM) TECHNAI G^2 20, with 200 kV accelerating voltage. Diffused reactance spectra were recorded with the Perkin Elmer Lambda 750 UV–vis NIR (ultraviolet-visible near-infrared) spectrometer. The Photoluminescence excitation and emission spectra of samples were studied by using the Perkin Elmer Photoluminescence spectrophotometer. To test the thermal stability the phosphor materials were heated outside and PL was measured. Finely, the Fluorolog-3 (Horiba Jobin Yvon) spectrofluorometer excited with PMT attached 25 W pulsed Xenon lamp in phosphorescence mode used for recording lifetime decay curves.

3. Result and discussion

3.1. X-ray diffraction characterization

The XRD profiles of $Ca_{0.5}Y_{1.90-x}O_3$:xHo^{3+} (x = 0.05, 1, 1.5, 2, 2.5, 3 mole%) samples were measured for 2θ = 10°−80° range and presented in Fig. 1**(a)**. Synthesized samples display high intensity and sharp peaks and refer to crystalline nature and are matched with the standard (JCPDS: 83–0928) data of Y_2O_3. All the phosphors have similar exhibit similar XRD pattern with the most intense XRD peaks are ~29.2°, 33.8°, 48.4°, 57.6° belongs to diffraction plane (222), (400), (440) and (622) plane, respectively. There are other peaks with low intensity that are also present and well matched with the JCPDS: 83–0928. This revealed samples are cubic structure with the $Ia\bar{3}$ (206) Space group. It has been observed that there is a small shift in XRD peaks (222) towards the higher angle side after doping with xHo^{3+} (x = 0.05, 1, 1.5, 2, 2.5, 3 mol%) (Fig. 1**(b)**). This shift in peak attributed to mismatch in radii of Y^{3+} (0.90 Å) and Ca^{2+} (1.1 Å) and Ho^{3+} (0.901 Å) during doping [14]. In the host ($Ca_{0.5}Y_{1.90-x}O_3$) the ionic radii of Ho^{3+} is similar with that of Y^{3+} hence doping with Ho^{3+} most likely replaces Y^{3+} as the dopant has tendency to substitute similar ionic radii. This replacement of Ho^{3+} into the Y^{3+} sites of $Ca_{0.5}Y_{1.90-x}O_3$ was also favoured by charge balancing. As the doping concentration of doped ions (Ca^{2+}, Ho^{2+}) are low, impurity peaks of other phases have been not found, but the intensity of the XRD peaks decreases with increasing the concentration of Ho^{3+}.

Further, the crystallite size of $Ca_{0.5}Y_{1.90-x}O_3$:xHo^{3+} phosphor has been estimated with Debye–Scherrer (D-S) formula and Williamson-Hall (W-H) relation given as [12,15]:

$$D = \frac{0.89\lambda}{\beta\cos(\theta)} \quad (1)$$

$$\beta Cos(\theta) = \frac{K\lambda}{D} + 4\varepsilon\, Sin(\theta) \quad (2)$$

where, λ is wavelength of x-ray (0.15,406 nm), θ is Bragg's angle of diffraction, β is the full width at half maxima, and ε is the strain present in the sample. The value of average crystallite size and strain present in the samples were calculated from the intercept and slope of the W-H plot given in Fig. 1**(c)**. The particle size of the Debye–Scherrer method is less compared to the W-H method. It might be due to the W-H method including lattice strain also during particle size calculation [11] . It has been observed that lattice strain increases with doping, this might be

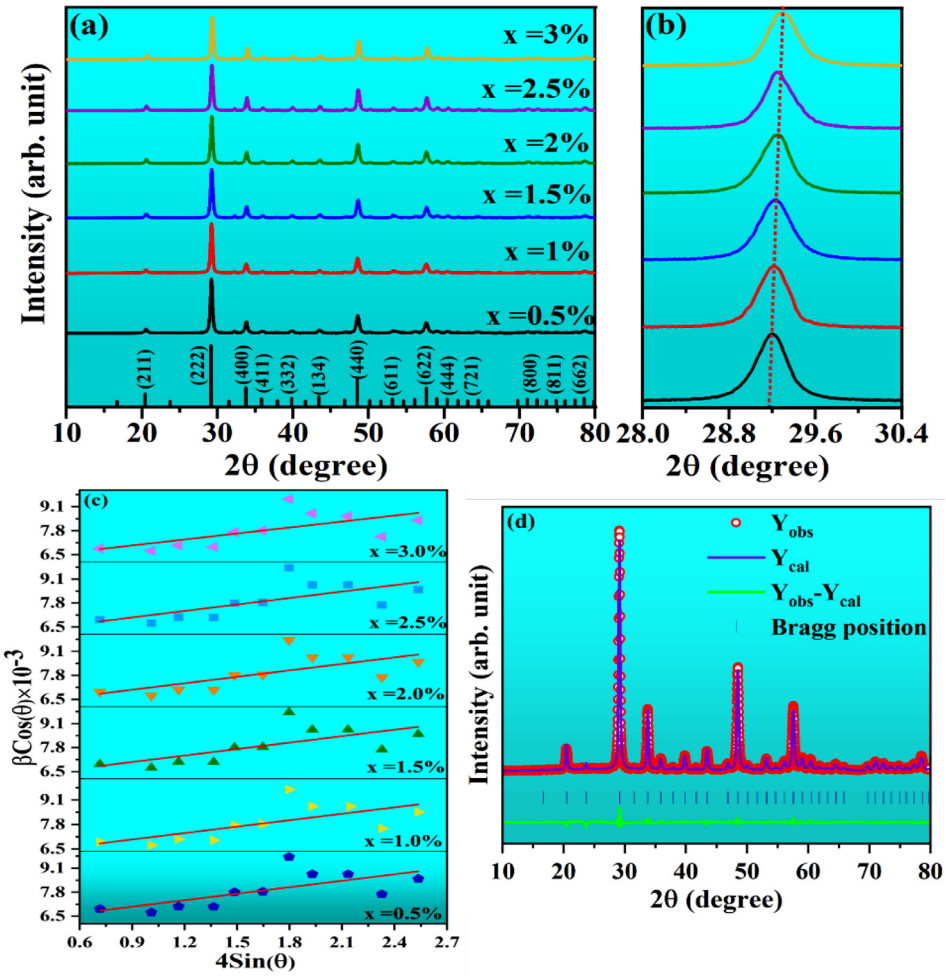

Fig. 1. **(a)** Powder XRD patterns and **(b)** magnified pattern of XRD for 28–30.4° **(c)** Hall–Williamson plot of $Ca_{0.5}Y_{1.90-x}O_3$:xHo^{3+} (x = 0.05, 1, 1.5, 2, 2.5, 3 mole%) phosphors **(d)** Rietveld refinement of $Ca_{0.5}Y_{1.90-x}O_3$:xHo^{3+} (2 mol%) nanophosphor.

Table 1
Structural parameters for $Ca_{0.5}Y_{1.90-x}O_3$:x$Ho^{3+}$with different concentration of Ho^{3+}.

Nanophosphor $Ca_{0.5}Y_{1.90-x}O_3$:xHo^{3+} (for X mole%)	Crystallite size D_{hkl} (nm)		microstrain $\varepsilon \times 10^{-3}$	Dislocation density (nm^{-2}) $\delta \times 10^{-4}$
	D-S formula	W-H plot		
Ho^{3+}=0.5	20.4	22.9	1.08	18.9
X = 1	20.9	23.1	1.13	18.6
X = 1.5	21.7	23.2	1.17	18.5
X = 2	22.9	23.2	1.17	18.5
X = 2.5	23.1	23.2	1.17	18.5
X = 3	23.8	24.2	1.18	17.0

due to doping with Ca^{2+}/ Ho^{3+} in Y_2O_3. With the average crystallite size calculated from Eq. (2) other structural parameter like microstrain ($\varepsilon = \frac{\beta Cos(\theta)}{4}$) and dislocation ($\delta = \frac{1}{D^2}$) [12] has been also estimated and values are given in Table 1. These results also show that the doping ion creates a little distortion in the Y_2O_3 crystal field but does not affect the cubic phase of it.

Furthermore, the effect of doping of Ca^{2+}/ Ho^{3+} with Y_2O_3 on the lattice constants and cell volume has been calculated from XRD data through Rietveld refinement using FullProf software for 2 mol% doping of Ho^{3+} ions (Fig. 1**(d)**). The Goodness of Fit (GOF) ($GOF = \chi^2 = (R_p/R_{wp})^2$) was found to be 1.74, this confirms good fitting between theoretical and experimental plots. Refinement also conforms the cubic phase with space group Ia $\underline{3}$ (206). Moreover, it has been estimated that doping increases lattice constant from 10.61 Å (JCPDS: 83–0928) to 10.62 Å and volume 1194 Å^3 to 1197.1 Å^3 for 2 mol% doping. This might be due to doping with comparatively bigger ions (Ca^{2+}/ Ho^{3+}) than Y^{3+} [15].

3.2. Morphological characterization

The surface morphology and particle size distribution of Ho^{3+} doped nanophosphor sample was investigated with TEM. Fig. 2 depict the TEM image of 2 mol% Ho^{3+} doped $Ca_{0.5}Y_{1.90-x}O_3$:xHo^{3+}nanophosphor. It can be seen from the TEM (Fig. 2**(a)**) image that particles are in the nanometre range. These particles have small average crystallites size ~21 nm (Fig. 2**(b)**) with irregular in shape and slightly agglomerated. Here, in the present study, urea has been used as a fuel which may expedite the nucleation of particles, thereby resulting in the agglomerates after combustion synthesis [16,17]. It has been also observed that average particle size values are consistent with the estimated values from the XRD pattern using scherrer's equation. The HRTEM image given in Fig. 2**(c)** show that the distance between the fringes is 0.305 nm, this can be allocated to (222) plane of crystal [8]. The SAES pattern (Fig. 2**(d)**) also shows the crystalline nature of $Ca_{0.5}Y_{1.90-x}O_3$:x$Ho^{3+}$and index with (222), (400), (440), (622) plane [18,19]. In SAED pattern several diffraction spots, these spots are ordered in ring form which resemble to high nano crystallinity with polycrystalline nature of sample.

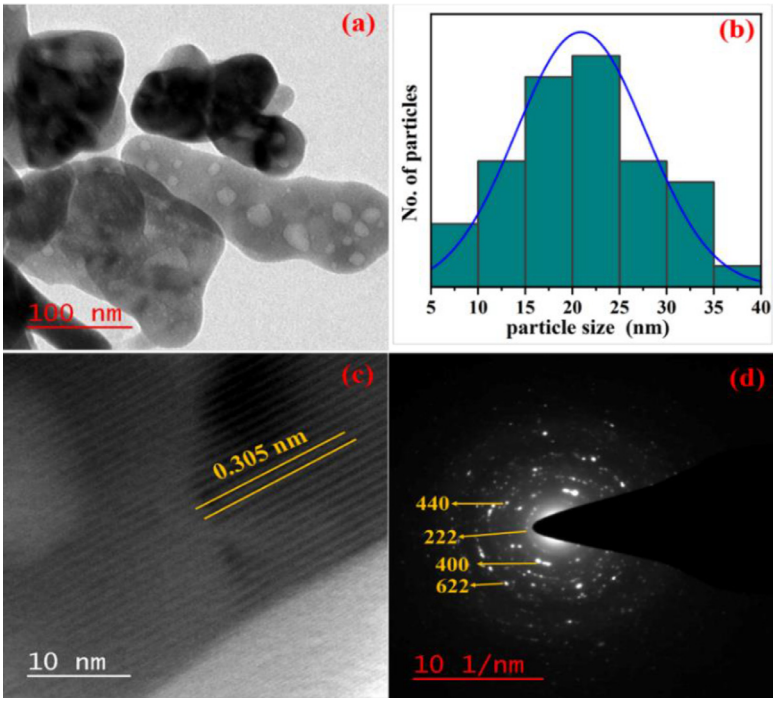

Fig. 2. **(a)** TEM image **(b)** particle distributions histogram **(c)** lattice fringes **(d)** SAED analysis of $Ca_{0.5}Y_{1.90-x}O_3$:xHo^{3+} (2 mole%) nanophosphor.

3.3. Fourier transform- infrared (FT-IR)

FT-IR spectra are generally used to identify organic and inorganic functional groups attached with the prepared samples for the range 500 cm^{-1} to 4000 cm^{-1} given in the Fig. 3. Which clearly confirms the absorption band of Y-O starching near 558 cm^{-1} [19]. The band near 855 cm^{-1} confirms the C–O vibration of CO_3^{2-} and absorption near 1433 cm^{-1} represents symmetric and asymmetric vibrations of C–O group. The presence of this group may be due to absorption due to atmosphere or residue carbon remaining during synthesis [20]. With this, the band centered at 3400–3600 cm^{-1} and 1500 cm^{-1} display starching and bending vibrations of -OH group [9]. It can be seen that no other residual peaks are present hence, this indicates pure phase formation of samples.

3.4. Diffuse reflectance spectra (DRS) characterization

The diffuse reflectance spectra of $Ca_{0.5}Y_{1.90-x}O_3$:x$Ho^{3+}$is shown in Fig. 3**(a)**, for the range 200-700 nm. The dominant peak at ~220 nm is accredited to host absorption, with this there are several less intense peaks at 360 nm, 448 nm, 463, 540, and 648 nm are corresponding to $^3H_6$, $^5G_6$, $^5F_3$+$^3K_8$, $^5F_4$+$^5F_3$, $^5S_2$, and$^5F_5$ transition of Ho^{3+} ions. These peaks are arising due to 4f-4f electronic transitions from ground state ($^5I_8$) to upper excited states of Ho^{3+} ions [5,8]. This result confirms the successful doping of Ho^{3+} in $Ca_{0.5}Y_{1.90-x}O_3$ host. Further, the optical bandgap of $Ca_{0.5}Y_{1.90-x}O_3$:xHo^{3+} was calculated with the Tauc's equation from the Tauc plot given in Fig. 3 **(b & c)** [6,11].

$$\alpha h\nu = C(h\nu - E_g)^n \quad (3)$$

where, C is proportionality constant and hν is photon energy, α is the absorption coefficient, E_g is the energy of optical band gap. The value of 'n' is different for different transitions as ½ for direct allowed, 3/2 for direct forbidden, 2 indirect allowed and 3 for indirect forbidden transition, respectively. Here, we consider direct and indirect allowed transitions so in this case the value of 'n' is ½ and 2 [18]. The optical band gap E_g was calculated by plotting hν verses $(\alpha h\nu)^n$ by extrapolating the linear region of the plot up to α =0. The estimated values for energy band gap of direct allow transition are 5.74, 5.72, 5.71, 5.78, 5.69, 5.07 eV and for indirect allow transition are 5.0, 5.02, 5.00, 4.90, 4.91, 4.99 eV for different concentration of Ho^{3+} ions x = 0.5, 1, 1.5, 2, 2.5, 3 mol%, respectively. This high value indicates host material has excellent PL properties [6]. It has been observed that there is slight variation of energy band gap for direct and indirect transitions with increase of Ho^{3+} ion concentration; this variation in band gap is also mentioned by Raman et al. [4].

3.5. Photoluminescence (PL) analysis

The photoluminescence excitation spectra of $Ca_{0.5}Y_{1.90-x}O_3$:xHo^{3+} with different concentration of Ho^{3+} (x = 0.05, 1, 1.5, 2, 2.5, 3 mole%) were given in Fig. 4**(a)**, which was recorded for the range 320-500 nm. The spectra are monitored for the emission wavelength λ_{em} = 551 nm, and contains several peaks at 336 nm ($^5I_8 \rightarrow {}^3F_4$, 345 nm ($^5I_8 \rightarrow {}^3L_9$), 361 nm ($^5I_8 \rightarrow {}^3H_5$), 374 nm ($^5I_8 \rightarrow {}^5G_4$), 448 nm ($^5I_8 \rightarrow {}^5G_6$), 459 nm ($^5I_8 \rightarrow {}^3K_8$), 460 nm ($^5I_8 \rightarrow {}^5F_2$) and 484 nm ($^5I_8 \rightarrow {}^5F_3$) correspond to the transitions. These excitation peaks are arisen due to f-f transitions from ground state of Ho^{3+} to various excited states [4] similar, type of transition was also mentioned and reported in Singh et al. [6]. Amongst these transitions, the 448 nm ($^5I_8 \rightarrow {}^3G_6$) is most instance, hence chosen for recording the excitation of the sample.

The PL emission spectra of $Ca_{0.5}Y_{1.90-x}O_3$:xHo^{3+} recorded for the excitation wavelength at λ_{ex}= 448 nm for the 500-700 nm wavelength has been presented in Fig. 4**(b)**. The emission peaks consist three emissions at 539 nm ($^5F_4 \rightarrow {}^5I_8$) and 551 nm ($^5S_2 \rightarrow {}^5I_8$) lie in strong green region and a weak peak at 670 nm ($^5F_5 \rightarrow {}^5I_8$) in red region which are characteristic peaks of Ho^{3+} and confirms the presence of Ho^{3+} ion in the synthesized samples [21]. It can be seen that ($^5S_2 \rightarrow {}^5I_8$) transitions at 551 nm is dominant over the other transitions in $Ca_{0.5}Y_{1.90-x}O_3$:xHo^{3+} nanophosphor. Hence it can be said that in all the transitions, ($^5S_2 \rightarrow {}^5I_8$) transition is most instance which lie in green region of visible light spectra. Further the effect of doping concentration on the PL emission intensity has been observed as given in Fig. 5**(a)**.

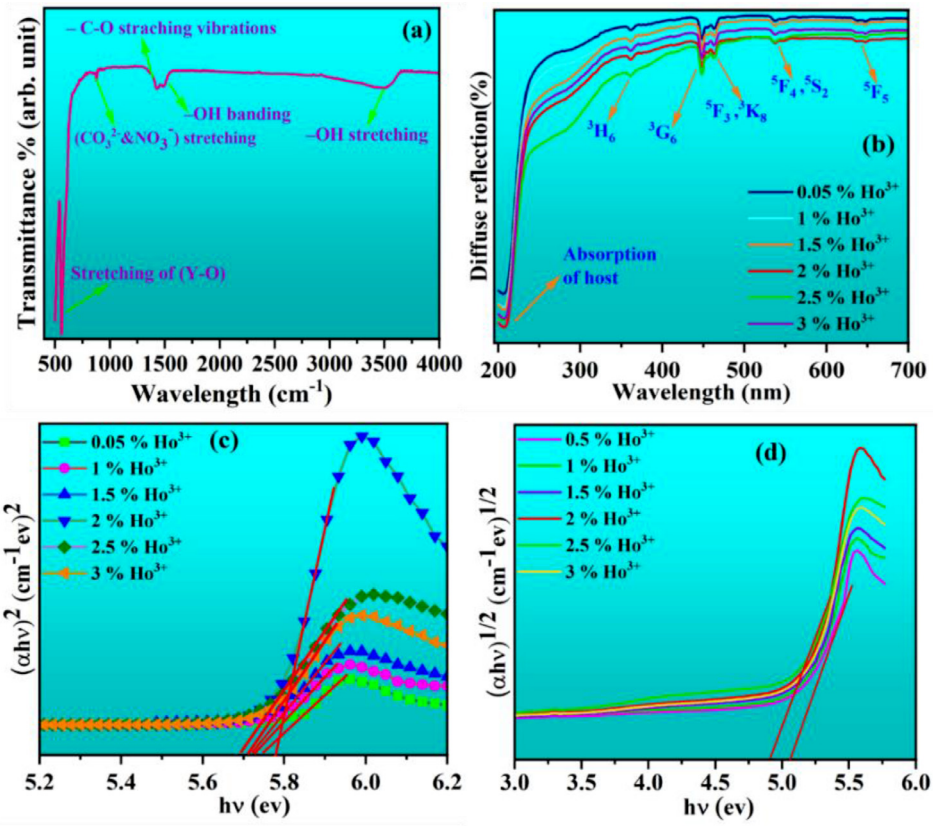

Fig. 3. **(a)** FT-IR spectrum of $Ca_{0.5}Y_{1.90-x}O_3$:xHo^{3+} (2 mole%) nanophosphor **(b)** UV-Vis diffuse reflectance spectra **(c)** Tauc plot of $(\alpha h\nu)^2$ verses hν and **(d)** $(\alpha h\nu)^{1/2}$ verses hν of $Ca_{0.5}Y_{1.90-x}O_3$:xHo^{3+} for different concentrations of Ho^{3+}.

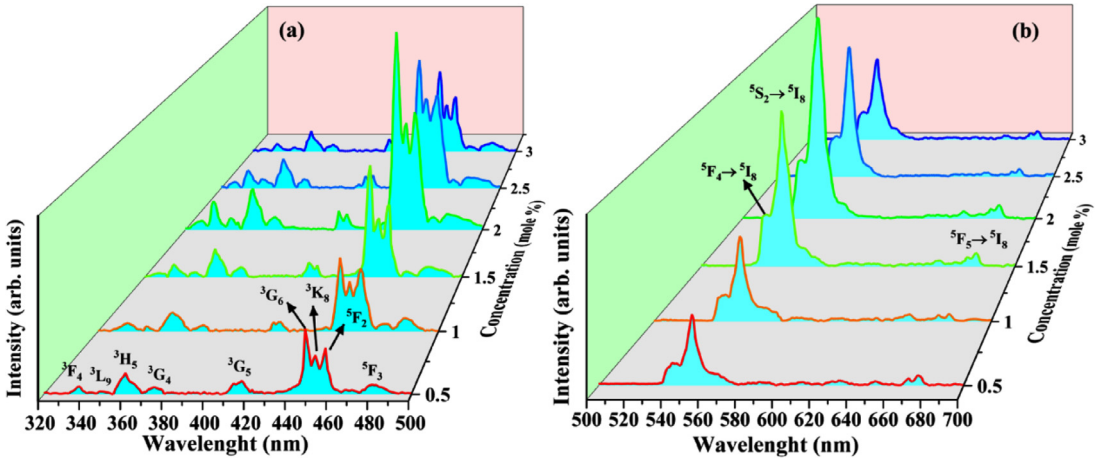

Fig. 4. **(a)** Excitation spectra of under λ_{em} = 551 nm **(b)** emission spectra under λ_{ex}= 448 nm of $Ca_{0.5}Y_{1.90-x}O_3$:xHo^{3+} (x = 0.5, 1, 1.5, 2, 2.5, 3 mole%) phosphors.

It has been seen that intensity increases up to 2 mol% and further decreases with increasing concentration of Ho^{3+}, and this owing to concentration quenching effect [5]. The phenomena of concentration quenching can be elucidated in two ways; one of them is due to presence of defects and impurity ions in the crystal lattice and causes energy transfer through the lattice vibration and leads to concentration quenching. In the second process, excited state energy transfer arises through cross relaxation/nonradiative transitions and this phenomenon is strongly influenced by doped ion concentration[4, 6]. This energy transfer mechanism through cross-relaxation/nonradiative transitions process may be understood by the energy level diagram given in Fig. 6. The non-radiative energy transfer is also one of the reasons for the concentration quenching. This might be due to when Ho^{3+} ion concentration is increased then they become close enough to each other or forms agglomerated structure, which leads to effective energy transfer through energy transfer and non-radiative cross-relaxation between Ho^{3+} ions and reduces the PL intensity efficiently [4]. Hence, the 2 mol% is considered as an optimal concentration of Ho^{3+} ion in $Ca_{0.5}Y_{1.90-x}O_3$:xHo^{3+} nanophosphor.

3.6. Energy transfer studies of $Ca_{0.5}Y_{1.90-x}O_3$:xHo^{3+} nanophosphor

Further, in order to understand the energy transfer mechanism, the critical distance between the Ho^{3+}-Ho^{3+} ions can be calculated

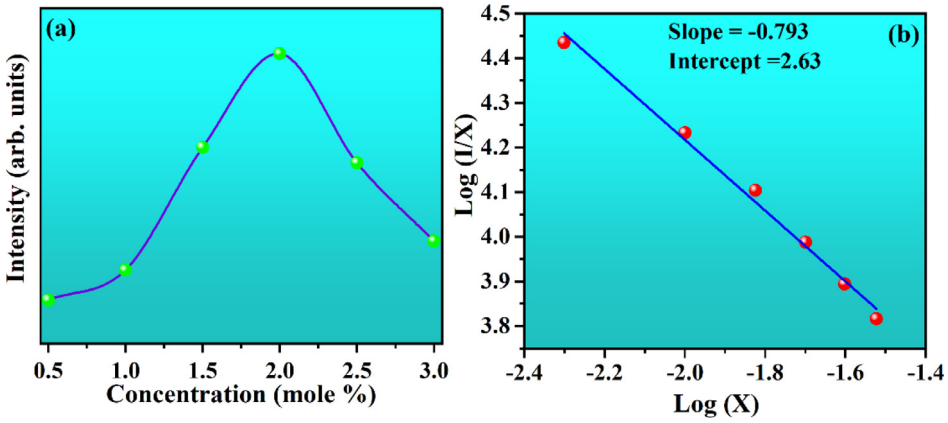

Fig. 5. **(a)** Variation of emission intensity 551 nm ($^5S_2 \rightarrow {}^5I_8$) and **(b)** plot of log(I/x) vs. log(x) in $Ca_{0.5}Y_{1.90-x}O_3$:xHo^{3+} at different concentration of Ho^{3+} ions.

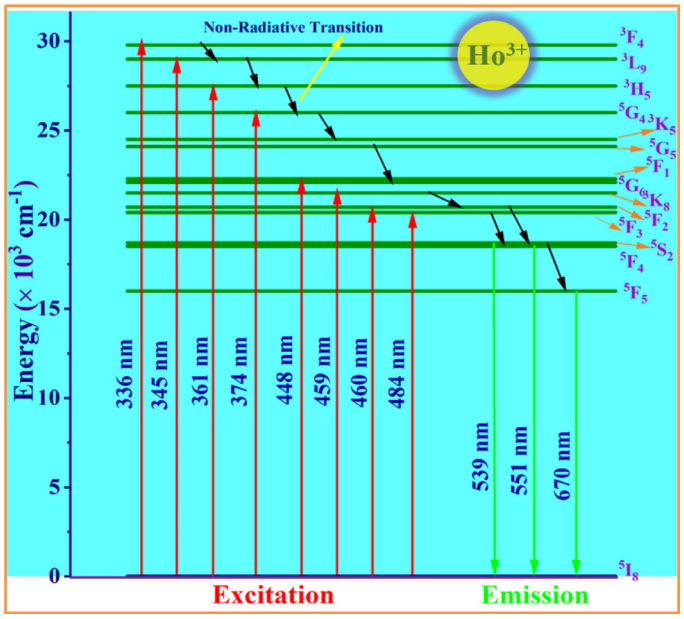

Fig. 6. Schematic energy level diagram showing excitation and emission of Ho^{3+} in $Ca_{0.5}Y_{1.90-x}O_3$:xHo^{3+} nanophosphor.

by Blasse's equations **(4)** [22,23]:

$$R_c \approx 2\left[\frac{3V}{4\pi N X_c}\right]^{1/3} \tag{4}$$

where V is volume of unit cell, N is occupancy number per unit cell in the host matric and X_c is Critical concentration of dopant ion at which emission intensity is maximum. If the critical distance between ions is less than 5 Å then non-radiative energy transfer occurs and if it is more than 5 Å then multipolar interaction arises [24]. In this case, $V = 1197.1$ Å^3, $X_c = 2$ mol% and $N = 16$ and the calculated value of R_c is found 19.26 Å, which is greater than 5 Å. This value shows that the energy transfer in this case is due to multiple interactions. Furthermore, there are three types of multipole interactions, which are dipole-dipole interaction (d-d), dipole-quadrupole interaction (d-q) and quadrupole-quadrupole interactions (q-q). In all these interactions the dominant one can be recognized through Dexter's Eq. (5) [4,25]:

$$\frac{I}{X} = \frac{K}{\left[1+\beta(X)^{\frac{Q}{3}}\right]} \tag{5}$$

where, (I/X) is the emission intensity per unit activator ion concentration (Ho^{3+}), β and K are constant for the given excitation condition of phosphor material and Q indicates type of interactions. When the values of Q are 3, 6 represents dipole – dipole interaction, 8 for dipole-quadrupole and 10 for quadrupole - quadrupole interactions [26]. Fig. 5**(b)** represents the plot between Log (X) versus Log (I/X) on logarithmic scale. The plot is fitted linearly and the value of slope is −0.793, which is equal to -Q/3. Therefore, the type of interaction a in this case Q ~2.1 and it is closer to 3 which recommend dipole -dipole type interaction. Hence in this case dipole-dipole interactions are responsible for energy transfer and subsequently for the PL quenching of Ho^{3+} ions in $Ca_{0.5}Y_{1.90-x}O_3$:xHo^{3+} nanophosphor.

3.7. Decay curve analysis

The lifetime decay curve of Ho^{3+} ions for the $^5S_2$ state for different concentrations has been observed with 488 nm excitation and 551 nm emission wavelength given in Fig. 7**(a–f)**. The decay curve was well fitted with the single exponential curve $I(t) = I_0 exp(-\frac{t}{\tau})$ where, I_0 and I(t) is the initial emission intensity and at 0 s. and t sec., and τ is the lifetime [27,28]. The lifetime values of $Ca_{0.5}Y_{1.90-x}O_3$:xHo^{3+} phosphors for different concentration (x = 0.05, 1, 1.5, 2, 2.5, 3 mole%) of Ho^{3+} is found to be 1.08, 1.13, 1.29, 1.35, 1.21, 1.10 ms, respectively. It can be noted that the PL lifetime of $Ca_{0.5}Y_{1.90-x}O_3$:xHo^{3+} energy level gradually increases from 1.08 to 1.35 ms with increase of concentration of Ho^{3+} from 0.5 to 2 mole%. However, lifetime value decreases further increase of concentration, this attributed to the non-radiative energy transfer and concentration quenching effect [29]. As we know, with the increase of Ho^{3+} ions concentration, the distance between doped ions decreases which leads to increase of non-radiative energy transfer probability between Ho^{3+} ions and is responsible for decrease of lifetime [22]. The increase in lifetime values with concentration results supports PL emission spectra.

3.8. Thermal stability of $Ca_{0.5}Y_{1.90-x}O_3$:xHo^{3+} nanophosphor

As we know thermal stability vastly influences the lifetime, CIE and output light of the LEDs, and also for validation of feasibility of the prepared nanophosphor for commercial application thermal stability should be known. The temperature dependent PL spectra of the $Ca_{0.5}Y_{1.90-x}O_3$:$2.0Ho^{3+}$ phosphor measured with 448 nm excitation for 300 -510 K range as given in Fig. 8**(a&b)**. It can be seen that with increase of temperature the emission intensity decreases owing to non-radiative phonon relaxation from higher levels via crossover process. As the temperature increases 510 K emission intensity decreases up to 72%. Further, to inspect thermal stability of

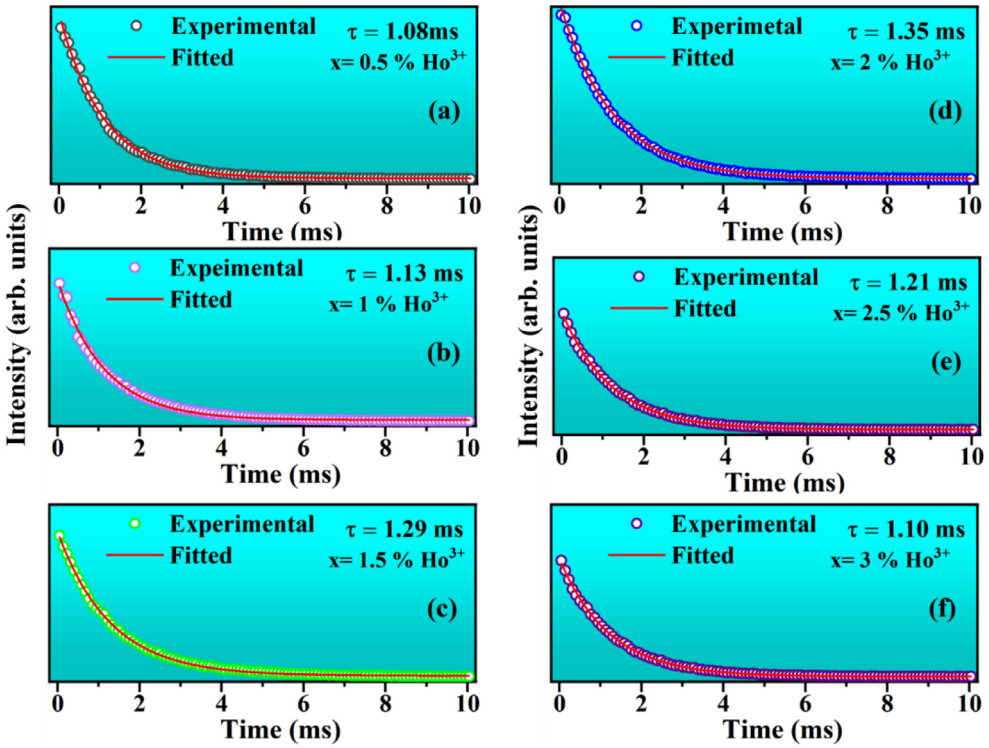

Fig. 7. Luminescence decay curve of $Ca_{0.5}Y_{1.90-x}O_3$:xHo^{3+} phosphors with different concentration of Ho^{3+} ions.

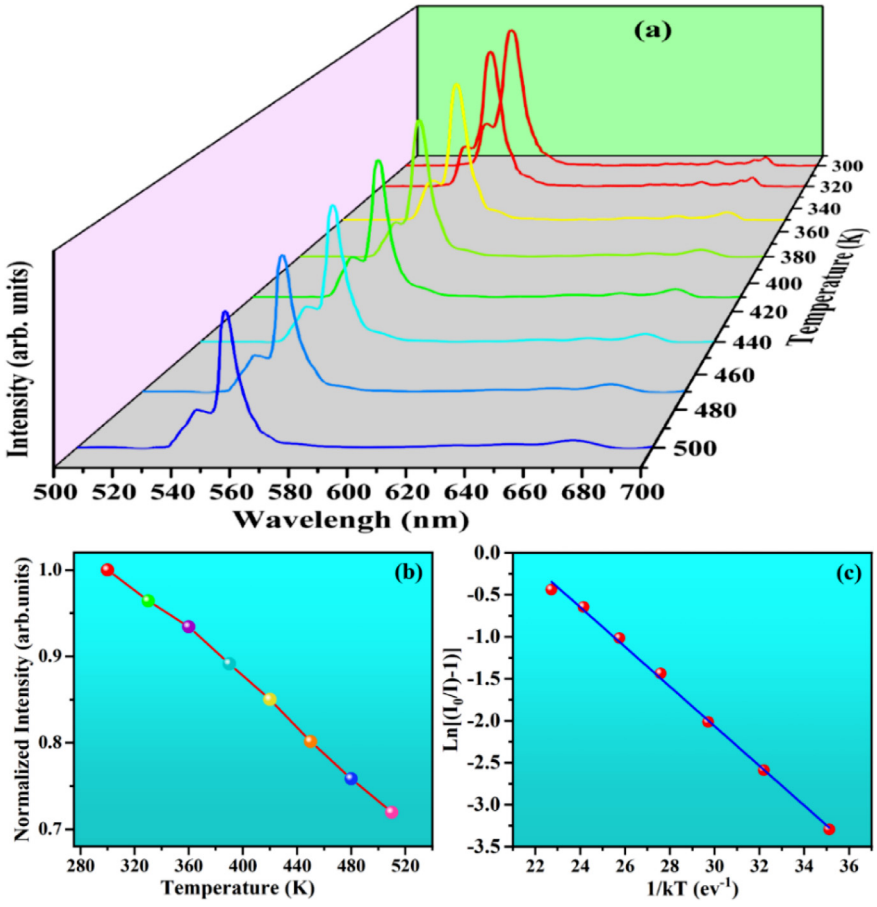

Fig. 8. (a) & (b) PL emission spectra as a function of temperature for $Ca_{0.5}Y_{1.90-x}O_3$:$2.0Ho^{3+}$ nanophosphor **(c)** Arrhenius plot of ln $[(I_0/I)-1]$ versus 1/kT for thermal quenching nature of $Ca_{0.5}Y_{1.90-x}O_3$:$2.0Ho^{3+}$sample.

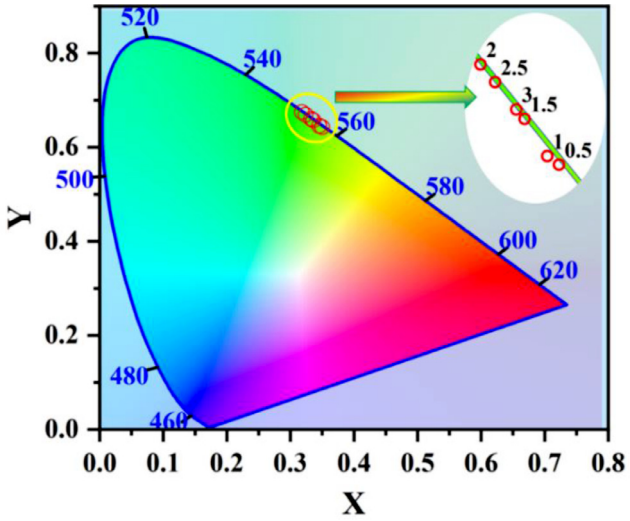

Fig. 9. The CIE 1931 chromaticity diagram of $Ca_{0.5}Y_{1.90-x}O_3$:xHo^{3+} (x = 0.05, 1, 1.5, 2, 2.5, 3 mole%) phosphors.

the phosphor Arrhenius Eq. (6) has been employed to calculate the activation energy [27,30]:

$$\ln\left(\frac{I_0}{I}-1\right)=\ln A-\frac{\Delta E}{kT} \quad (6)$$

where, I_0 and I initial emission intensity and intensity at different temperatures, k is Boltzmann constant, A is constant and ΔE is ascribed as activation energy. According to Arrhenius equation ln [(I_0/I)−1] versus 1/kT plot (Fig. 8**(c)**) has been plotted, and fitted linearly with the slope −0.237 eV. The slope of this plot gives activation energy, therefore ΔE the thermal quenching is estimated as 0.237 eV. Hence the $Ca_{0.5}Y_{1.90-x}O_3$:2.0Ho^{3+} nanophosphor has good thermal stability and can be used for the LEDs fabrication.

3.9. Photometric analysis

To recognize the purity in emitted color of the synthesised nanophosphor, the color coordinate was investigated with the CIE 1931 (Commission International de l′Eclairage). The CIE coordinated with different concentrations of $Ho^{3+}$was estimated with the emission data presented in Fig. 9. The CIE coordinates for different concentrations of Ho^{3+} given in Table 2. It can be seen that color coordinates lie in the bright green spectral region which well match with the PL results. Hence, the $Ca_{0.5}Y_{1.90-x}O_3$:xHo^{3+} nanophosphor might be used for the solid-state lighting device to give emission in the green region. Further, the percentage color purity exhibited by the $Ca_{0.5}Y_{1.90-x}O_3$:xHo^{3+} can be estimated through the formula (7) [6,31]:

$$Color\ purity=\frac{\sqrt{\sqrt{(x-x_w)^2+(y-y_w)^2}}}{\sqrt{\sqrt{(x_w-x_d)^2+(y_w-y_d)^2}}}\times 100\ \% \quad (7)$$

Table 2
The CIE coordinates, CCT coordinate, CCT values,% color purity and CIR value of $Ca_{0.5}Y_{1.90-x}O_3$:xHo^{3+} nanophosphors with distinct concentration of Ho^{3+}.

$Ca_{0.5}Y_{1.90-x}O_3$:xHo^{3+} Nanophosphor (at. mole%)	CIE coordinates (x, y)		CCT value (K)	Color purity (%)	CRI
0.5	0.349	0.643	5260	90	98.50
1	0.344	0.645	5330	91	98.49
1.5	0.335	0.657	5467	94	98.44
2	0.317	0.675	5724	98	98.36
2.5	0.321	0.669	5639	97	98.39
3	0.332	0.660	5516	95	98.42

where, (x,y) present the color coordinates of sample point, (x_w,y_w) denote the coordinate of the illuminant point (x_w = 0.3101, y_w = 0.3162) and (x_d,y_d) represents the coordinated of the dominant wavelength (x_d = 0.318, y_d = 0.676). The calculated values of color purity values are given in Table 2, these values obtained indicate high purity of green emission in nanophosphor.

Furthermore, the correlation color temperature (CCT), the values have been calculated as CCT present the quality of light source and it is used to show cool and warm nature of light. The CCT values can be estimated by McCamy's empirical formula (8) [4,32]:

$$T=-499n^3+3525n^2-6823.3n+5520 \quad (8)$$

where, $n=\frac{x-0.332}{y-0.186}$ and x, y is CIE coordinated. The obtained CCT values of $Ca_{0.5}Y_{1.90-x}O_3$:xHo^{3+} nanophosphors are given in Table 2. All the CCT values are greater than 3000, which show these lies in the cool light region and can be said that it is a stable material with prodigious use for cool LEDs and display applications [33,34]. Color purity of the prepared phosphor samples was also estimated and tabulated in Table 2. The samples display high color purity and the green color purity reached maximum 98% for the 2 mol% doped $Ca_{0.5}Y_{1.90-x}O_3$:xHo^{3+} nanophosphors.

3.10. Quantum efficiency (QE)

With the color purity, chromatic properties, thermal stability quantum efficiency is one of the important parameters of the synthesised nanophosphor to reorganize their applicability for LEDs applications. The quantum efficiency (η) of the optimized $Ca_{0.5}Y_{1.90-x}O_3$:Ho^{3+} (2 mole%) has been estimated by following method (9) [35,36]:

$$QE(\eta)=\frac{number\ of\ photons\ emitted\ (\varepsilon)}{number\ of\ photons\ absorbed\ (\alpha)}=\frac{E_c-E_a}{L_a-L_c} \quad (9)$$

where, E_c is the integrated luminescence of the phosphor caused by direct excitation, E_a is the integrated luminescence from the empty integrating sphere (without sample), L_a is the integrated excitation profile from the empty integrating sphere, and L_c is the integrated excitation profile when the sample is directly excited by the incident beam. The QE of the sample with λ_{ex}= 448 nm excitation wavelength was evaluated by integrated emission count for 500-700 nm range. The value has found to be ~81.1%. It is evident that the estimated value of the QE in this case is higher and comparable with the other green emitting phosphor, such as in case of Ho^{3+} doped $Ba_{0.65}Sr_{0.35}TiO_3$ (~57%) [37], $YAlO_3$:Ho^{3+} (~61%) [36], and Ho^{3+}:LaF_3 (~55.8%) [38]. This result indicates that the $Ca_{0.5}Y_{1.90-x}O_3$:Ho^{3+} (2 mole%) nanophosphors are promising for the LEDs.

4. Conclusion

Our study reports the successful synthesis of $Ca_{0.5}Y_{1.90-x}O_3$:xHo^{3+} with different concentrations of Ho^{3+} ions (x = 0.5, 1, 1.5, 2, 2.5, 3 mole%) nanophosphor through solution combustion method. XRD reveal the cubic phase with the $Ia\bar{3}$ (206) Space group and Transmission electron microscope (TEM) confirms the irregular shape particle in nanometre range ~21 nm, respectively. The band gap estimated by Tauc's equation is 5.78 eV, 4.90 eV for direct and indirect band gaps for 2 mol% of Ho^{3+}, respectively. The PL excitation spectra show numerous peaks corresponding to f-f transitions of Ho^{3+} for 551 nm emission. The PL emission spectra shows strong green correspond to $^5S_2 \rightarrow {}^5I_8$ (551 nm) transition of Ho^{3+} ions. The critical concentration of Ho^{3+} in $Ca_{0.5}Y_{1.90-x}O_3$:xHo^{3+} was detected as 2 mol% above this concentration quenching effect has been observed. The

$Ca_{0.5}Y_{1.90-x}O_3$:2.0Ho^{3+}green emitting phosphor shows excellent thermal stability with activation energy 0.27 eV. Photometric properties have been also obtained using chromaticity diagram for the optimal concentration (2 mol%) as CIE coordinates (0.317, 0.675), CCT (5724 K), color purity (98%), CRI (98.36%) and quantum efficiency (~81.1%). The various characterization studies manifested strong green emission (at 551 nm) of $Ca_{0.5}Y_{1.90-x}O_3$:xHo^{3+} nanophosphor which can be used for developing green emitting LEDs and display devices.

Declaration of Competing Interest

We confirm that this work is original and has not been submitted/published elsewhere. The article is exclusively submitted to **"Journal of Molecular Structure"**. We have no conflict of interest associated with this publication and there has been no significant financial support for this work that would have influenced its outcome. As a corresponding Author, I confirm that the manuscript has been read and approved for submission by all the named authors.

CRediT authorship contribution statement

Arpita Dwivedi: Methodology, Conceptualization, Data curation, Visualization, Validation, Writing – original draft, Writing – review & editing. **Monika Srivastava:** Formal analysis, Validation. **S.K. Srivastava:** Conceptualization, Validation, Supervision, Visualization.

Acknowledgments

The author (AD) gratefully acknowledges University Grants Commission (UGC), India for providing research fellowship. MS conveys their acknowledgement to DST, New Delhi (SR/WOS-A/CS-52/2018) for the WOS fellowship. SKS is thankful to the Institute of Eminence (IOE), BHU for financial support. Authors also gratefully acknowledged Prof. S.B. Rai BHU, Varanasi for the valuable suggestions and PL lifetime measurements.

References

[1] P. Kaur, A. Kaur, S. Singh, L. Singh, Investigation on structural and thermoluminescence properties of Ho^{3+} doped SrB_4O_7 phosphor for dosimetry applications, J. Mol. Struct. 1248 (2022) 131500.
[2] L. Melato, O. Ntwaeaborwa, R. Kroon, T. Motaung, S.V. Motloung, Effect of Ho^{3+} concentration on the structure, morphology and optical properties of $Ba_{0.5}Mg_{0.5}Al_2O_4$ nanophosphor, J. Mol. Struct. 1176 (2019) 217–225.
[3] N. Singh, V. Singh, S. Watanabe, J. Chubaci, T.G. Rao, H. Gao, P. Mardina, Studies of defects and optical properties of $CaAl_{12}O_{19}$: Ho^{3+} phosphor material, J. Alloys Compd. 663 (2016) 235–242.
[4] T.R. Raman, Y. Ratnakaram, Effect of Ho^{3+} ion concentration on structure and spectroscopic properties of $LiPbB_5O_9$: Ho^{3+} phosphor, J. Mol. Struct. (2021) 130759.
[5] V. Singh, K. Dabre, S. Dhoble, G. Lakshminarayana, Green emitting holmium (Ho) doped yttrium oxide (Y_2O_3) phosphor for solid state lighting, Optik (Stuttg) 206 (2020) 164339.
[6] V. Singh, C.B.A. Devi, S. Kaur, A. Rao, N. Singh, Optical properties of $Sr_2La_8(SiO_4)_6O_2$ doped with Ho^{3+} phosphor, Optik (Stuttg) (2021) 167268.
[7] Y. Guo, D. Wang, Y. He, Fabrication of highly porous Y_2O_3: Ho, Yb ceramic and its thermometric applications, J. Alloys Compd. 741 (2018) 1158–1162.
[8] T.S. Atabaev, H.H.T. Vu, Y.D. Kim, J.H. Lee, H.K. Kim, Y.H. Hwang, Synthesis and luminescence properties of Ho^{3+} doped Y_2O_3 submicron particles, J. Phys. Chem. Solids 73 (2) (2012) 176–181.
[9] H. Shi, X.Y. Zhang, W.L. Dong, X.Y. Mi, N.L. Wang, Y. Li, H.W. Liu, Effect of co–doped metal caions on the properties of Y_2O_3: Eu^{3+} phosphors synthesized by gel-combustion method, Chin. Phys. B 25 (4) (2016) 047802.
[10] D. Kumar, M. Sharma, O. Pandey, Effect of co-doping metal ions (Li+, Na+ and K+) on the structural and photoluminescent properties of nano-sized Y_2O_3: Eu^{3+} synthesized by co-precipitation method, Opt. Mater. (Amst) 36 (7) (2014) 1131–1138.
[11] A. Dwivedi, M. Srivastava, A. Srivastava, S. Srivastava, Synthesis of high luminescent Eu^{3+} doped nanoparticle and its application as highly sensitive and selective detection of Fe^{3+} in real water and human blood serum, Spectrochim. Acta Part A Mol. Biomol. Spectrosc. 260 (2021) 119942.
[12] P. Kumari, J. Manam, Enhanced red emission on co-doping of divalent ions (M^{2+}= Ca^{2+}, Sr^{2+}, Ba^{2+}) in YVO_4: Eu^{3+} phosphor and spectroscopic analysis for its application in display devices, Spectrochim. Acta Part A Mol. Biomol. Spectrosc. 152 (2016) 109–118.
[13] Ž. Antić, V. Lojpur, M.G. Nikolić, V. Đorđević, P.S. Ahrenkiel, M.D. Dramićanin, Strong emission via up-conversion of Gd_2O_3: Yb^{3+}, Ho^{3+} nanopowders co–doped with alkali metals ions, J. Lumin. 145 (2014) 466–472.
[14] V. Singh, C.B. Annapurna Devi, S. Kaur, A.S. Rao, N. Singh, Optical properties of $Sr_2La_8(SiO_4)_6O_2$ doped with Ho^{3+} phosphor, Optik (Stuttg) 242 (2021) 167268.
[15] J.B. Prasanna kumar, G. Ramgopal, Y.S. Vidya, K.S. Anantharaju, B. Daruka Prasad, S.C. Sharma, S.C. Prashantha, H.B. Premkumar, H. Nagabhushana, Bio-inspired synthesis of Y_2O_3: Eu^{3+} red nanophosphor for eco-friendly photocatalysis, Spectrochim. Acta Part A Mol. Biomol. Spectrosc. 141 (2015) 149–160.
[16] K. Tahmasebi, M.H. Paydar, The effect of starch addition on solution combustion synthesis of Al_2O_3–ZrO_2 nanocomposite powder using urea as fuel, Mater. Chem. Phys. 109 (1) (2008) 156–163.
[17] F. Deganello, A.K. Tyagi, Solution combustion synthesis, energy and environment: best parameters for better materials, Prog. Cryst. Growth Charact. Mater. 64 (2) (2018) 23–61.
[18] G. Ramgopal, Y. Vidya, K. Anantharaju, B.D. Prasad, S. Sharma, S. Prashantha, H. Premkumar, H. Nagabhushana, Bio-inspired synthesis of Y_2O_3: Eu^{3+} red nanophosphor for eco-friendly photocatalysis, Spectrochim. Acta Part A Mol. Biomol. Spectrosc. 141 (2015) 149–160.
[19] D. Kumar, A. Dwivedi, M. Srivastava, A. Srivastava, A. Srivastava, S. Srivastava, Gold nanorods modified Eu: Y_2O_3 dispersed PVA film as a highly sensitive plasmon-enhanced luminescence probe for excellent and fast non-enzymatic detection of H_2O_2 and glucose, Optik (Stuttg) 228 (2021) 166130.
[20] A.M. Khachatourian, F. Golestani-Fard, H. Sarpoolaky, C. Vogt, E. Vasileva, M. Mensi, S. Popov, M.S. Toprak, Microwave synthesis of Y_2O_3: Eu^{3+} nanophosphors: a study on the influence of dopant concentration and calcination temperature on structural and photoluminescence properties, J. Lumin. 169 (2016) 1–8.
[21] V. Singh, G. Lakshminarayana, A. Wagh, N. Singh, Luminescence features of green-emitting $CaLa4Si_3O_{13}$: Ho^{3+} phosphors, Optik (Stuttg) 207 (2020) 164284.
[22] P. Du, J.S. Yu, Eu $^{3+}$-activated La_2MoO_6-La_2WO_6 red-emitting phosphors with ultrabroad excitation band for white light-emitting diodes, Sci. Rep. 7 (1) (2017) 1–10.
[23] G. Dong, J. Zhao, M. Li, L. Guan, X. Li, A novel red Y_2MoSiO_8: Eu^{3+} phosphor with high thermal stability for white LEDs, Ceram. Int. 45 (2) (2019) 2653–2656.
[24] C.S. Kamal, T.V. Rao, P. Reddy, K. Sujatha, B.P. Ajayi, J.B. Jasinski, K.R. Rao, Unravelling the energy transfer mechanism in bismuth co-activation of $LaInO_3$: Sm $^{3+}$/Ho $^{3+}$ nanophosphor for color-tunable luminescence, RSC Adv. 7 (16) (2017) 9724–9731.
[25] A. Dwivedi, M. Srivastava, A. Dwivedi, A. Srivastava, A. Mishra, S. Srivastava, Synthesis and enhanced photoluminescence properties of red emitting divalent ion (Ca^{2+}) doped Eu: Y_2O_3 nanophosphors for optoelectronic applications, J. Rare Earths (2021).
[26] M. Letswalo, L. Reddy, A. Balakrishna, H. Swart, O. Ntwaeaborwa, Influence of $SO4^{2-}$ anionic group substitution on the enhanced photoluminescence behavior of red emitting $CaMoO_4$: Eu^{3+} phosphor, J. Alloys Compd. 854 (2021) 157022.
[27] J. Zhao, J. Dong, X. Ye, L. Wang, A promising novel red-emitting Eu^{3+}-activated neodymium calcium phosphate phosphor with good thermal stability and excellent color purity for WLEDs, J. Mol. Struct. 1240 (2021) 130567.
[28] A. Dwivedi, M. Srivastava, R. Upadhyay, A. Srivastava, R.S. Yadav, S.K. Srivastava, A flexible Eu:Y_2O_3-polyvinyl alcohol photoluminescent film for sensitive and rapid detection of arsenic ions, Microchem. J. 172 (2022) 106969.
[29] J. Yuan, W. Wang, Y. Ye, T. Deng, Y. Huang, S. Gu, Y. Chen, P. Xiao, 2.0 μm ultra broadband emission from Tm^{3+}/Ho^{3+} co-doped gallium tellurite glasses for broadband light sources and tunable fiber lasers, Crystals 11 (2) (2021) 190.
[30] H. Duan, R. Cui, X. Qi, C. Deng, Synthesis and photoluminescence of color tunable red emitting Ba_2YAlO_5: Eu^{3+} phosphors, J. Mol. Struct. 1205 (2020) 127551.
[31] R.K. Singh, S. Som, C.H. Lu, Spectroscopic investigation of red Eu^{3+} doped ceria nanophosphors and promising color rendition for warm white LEDs, J. Alloys Compd. 816 (2020) 152653.
[32] Y.J. Han, S. Wang, H. Liu, L. Shi, S.X. Liu, Y. Zhang, C. Liu, X.F. Shi, Q. Wang, Z.F. Mu, Z.Y. Mao, D.J. Wang, Z.W. Zhang, A novel promising red phosphor $Ca_9LiBi_{0.667}(PO_4)_7$:Eu^{3+} with excellent responsiveness to phytochrome PFR for the indoor plant cultivation, J. Mol. Struct. 1210 (2020) 127998.
[33] H. Gong, D. Yang, X. Zhao, E.Y.B. Pun, H. Lin, Upconversion color tunability and white light generation in Tm^{3+}/Ho^{3+}/Yb^{3+} doped aluminum germanate glasses, Opt. Mater. (Amst) 32 (4) (2010) 554–559.
[34] P. Sehrawat, P. Boora, M. Kumar, R. Malik, S. Khatkar, V. Taxak, Crystal structure engineering and optical analysis of novel greenish $Sr_9Al_6O_{18}$: Er^{3+} nanomaterials for NUV excitable cool-white LED applications, Chem. Phys. Lett. 759 (2020) 138044.

[35] K. Venkatachalaiah, H. Nagabhushana, G. Darshan, R. Basavaraj, B.D. Prasad, Novel and highly efficient red luminescent sensor based SiO_2@ Y_2O_3: Eu^{3+}, M+ (M+= Li, Na, K) composite core–shell fluorescent markers for latent fingerprint recognition, security ink and solid state lightning applications, Sens. Actuators B Chem. 251 (2017) 310–325.

[36] H. Premkumar, B. Ravikumar, D. Sunitha, H. Nagabhushana, S. Sharma, M. Savitha, S.M. Bhat, B. Nagabhushana, R. Chakradhar, Investigation of structural and luminescence properties of Ho^{3+} doped $YAlO_3$ nanophosphors synthesized through solution combustion route, Spectrochim. Acta Part A Mol. Biomol. Spectrosc. 115 (2013) 234–243.

[37] J. Wang, T. Zhang, R. Pan, Z. Ma, J. Wang, Spectroscopic and photoluminescence properties of Ho^{3+} doped $Ba_{0.65}Sr_{0.35}TiO_3$ nanocrystals, Phys. B Condens. Matter 407 (1) (2012) 160–164.

[38] H.M. Ha, T.T.Q. Hoa, N.N. Long, Radiative transition dynamics of holmium ions-doped LaF_3 nanocrystals, J. Mater. Sci. Mater. Electron. 29 (2) (2018) 1607–1613.